



1 **Machine learning-constrained projection of bivariate hydrological**
2 **drought magnitudes and socioeconomic risks**

3 Rutong Liu¹, Jiabo Yin^{1*}, Louise Slater², Shengyu Kang¹, Yuanhang Yang¹, Pan Liu¹, Jiali Guo^{3,4},
4 Xihui Gu⁵, Aliaksandr Volchak⁶

5 ¹State Key Laboratory of Water Resources Engineering and Management, Wuhan University, Wuhan,
6 Hubei, 430072, P.R. China

7 ²School of Geography and the Environment, University of Oxford, Oxford, UK

8 ³Engineering Research Center of Eco-environment in Three Gorges Reservoir Region, Ministry of
9 Education, China Three Gorges University, Yichang, Hubei 443002, China

10 ⁴College of Hydraulic and Environmental Engineering, China Three Gorges University, Yichang,
11 Hubei 443002, China

12 ⁵School of Environmental Studies, China University of Geosciences, Wuhan 430074, China

13 ⁶Engineering Systems and Ecology Faculty, Brest State Technical University, Moskovskaya 267,
14 224017 Brest, Belarus

15

16

17 *Correspondence: Jiabo Yin (jboyn@whu.edu.cn)

18



19 **Abstract**

20 Climate change accelerates the water cycle and alters the spatiotemporal distribution of hydrological
21 variables, thus complicating the projection of future streamflow and hydrological droughts. Although
22 machine learning is increasingly employed for hydrological simulations, few studies have used it to project
23 hydrological droughts, not to mention the bivariate risks of drought duration and severity as well as their
24 socioeconomic effects under climate change. We develop a cascade modeling chain to project future bivariate
25 hydrological drought characteristics in 179 catchments over China, using 5 bias-corrected GCM outputs
26 under three shared socioeconomic pathways, five hydrological models and a deep learning model. We
27 quantify the contribution of various meteorological variables to daily streamflow by using a random forest
28 model, then employ terrestrial water storage anomalies and a standardized runoff index to evaluate recent
29 changes in hydrologic drought. Subsequently, we construct a bivariate framework to jointly model drought
30 duration and severity by using Copula functions and the most likely realization method. Finally, we use this
31 framework to project future risks of hydrological droughts as well as associated exposure of gross domestic
32 product and population. Results show that our hybrid hydrological-deep learning model achieves >0.8 Kling-
33 Gupta efficiency in 161 out of 179 catchments. By the late 21st century, bivariate drought risk is projected to
34 double over 60% catchments, mainly located in Southwest China. Our hybrid model also projects substantial
35 GDP and population exposures by increasing bivariate drought risks, suggesting an urgent need to design
36 climate mitigation strategies towards a sustainable development pathway.



37 **1 Introduction**

38 In a warming world, the acceleration of the global water cycle is expected to alter the regional and
39 seasonal distribution of key hydrological variables such as precipitation and evapotranspiration (Allan et al.,
40 2020). As precipitation patterns are particularly sensitive to changes in atmospheric forcing and local
41 conditions, precipitation extremes are generally increasing globally, exacerbating spatial heterogeneity of
42 precipitation (Donat et al., 2016; Tabari, 2020). A suite of Shared Socioeconomic Pathways (SSPs) has been
43 proposed to simulate different possible future scenarios of societal responses to climate change, and these are
44 employed to investigate the possible effects of long-term climate change (Meinshausen et al., 2020; Zhang
45 et al., 2021). By using the SSP framework, numerous works have indicated that the redistribution of
46 precipitation may lead to the decline of water storage in some regions, and intensify water scarcity in arid
47 regions (Sönmez and Kale, 2018; Woolway et al., 2020; Yao et al., 2023). Under increasing atmospheric
48 greenhouse gases, numerous studies have reported a widespread increase in drought events, even in areas
49 with increasing annual runoff (Dai et al., 2018). The uneven distribution of precipitation and other
50 meteorological elements under climate change complicates predictions of future runoff and drought.

51 China's socioeconomic development, and particularly its agricultural sector, is threatened by the rapid
52 intensification of extreme hazards under climate change (Piao et al., 2010). Over the past years, China has
53 been hit by severe drought events which have caused considerable damage to ecosystem productivity and
54 socio-economic growth (Zhai and Zou, 2005; Yin et al., 2023). Water shortages, agricultural production, and
55 associated ecological degradation are key challenges hindering the sustainable development of the North
56 China Plain (Chen and Yang, 2013). Over the period of 1985-2014, drought accounted for about 19% of
57 economic losses among all meteorological hazards (Chen and Sun, 2019). With continuing global warming,
58 the economic losses from severe drought events might increase by over ten billions of US dollars per year by
59 the late 21st century (Su et al., 2018). For instance, one extreme drought in Sichuan Province in 2022 resulted
60 in power shortages and led to economic losses of 669 million dollars, underscoring the importance of
61 projecting future droughts over China (Lu et al., 2023).

62 Droughts can be triggered by divergent mechanisms, and are thus distinguished according to the type of
63 drought, such as meteorological and hydrological drought (Yihdego et al., 2019). The majority of studies
64 have focused on meteorological droughts, which can then be translated to a hydrological drought, while fewer
65 works have focused on hydrological drought probably due to lack of measurements like the standardized
66 runoff index (SRI) (Barker et al., 2016; Kumar et al., 2016; Tirivarombo et al., 2018). Furthermore,
67 hydrological droughts are not only affected by the water cycle but also by human interventions, which makes
68 them difficult to accurately be predicted (Wu et al., 2021). Currently, the majority of drought impact
69 assessments focus on the investigation of individual drought variables (i.e., drought duration, severity and
70 intensity, etc.) through univariate probabilistic models and stochastic theory (Myronidis et al., 2018;
71 Byakatonda et al., 2018; Zhang et al., 2022). However, univariate drought analysis cannot accurately describe



72 the probability of drought events, because droughts of either long duration or severe intensity can lead to
73 substantial socio-ecosystem damages (Castle et al., 2014; Udall and Overpeck, 2017). Therefore, the bivariate
74 framework based on Copula functions has been developed for drought projection, compensating for the
75 incompleteness of a single variable analysis (Ayantobo et al., 2017; Nabaei et al., 2019). At present, studies
76 on hydrological drought within a bivariate framework are still lacking. Beyond the choice of approach
77 (univariate or bivariate), the Gravity Recovery and Climate Experiment (GRACE) and GRACE-FO (GRACE
78 Follow-On) satellites now provide two decades of large-scale terrestrial water storage (TWS) data, which
79 captures the water deficit in various forms on land and can be used to monitor droughts (Schmidt et al., 2006).
80 The drought severity index based on TWS (TWS-DSI) can be used to monitor past drought events, which
81 also shows potential advantages in drought warning, forecasting, and projection (Nie et al., 2018; Pokhrel et
82 al., 2021).

83 In recent decades, many studies have used bias-corrected outputs from Global Climate Models (GCMs)
84 to project future hydrological drought scenarios (e.g., (Ashrafi et al., 2020; Kim et al., 2021; Dixit et al.,
85 2022)). The growing application of machine learning has revealed high potential for improving the accuracy
86 of hydrological simulation and prediction (Mokhtar et al., 2021). In recent years, many machine learning
87 algorithms have been adopted in drought simulation and produce a good performance, such as wavelet neural
88 networks (WNNs) (Xiuja et al., 2022), support vector machines (SVMs) (Zhu et al., 2021) and long short-
89 term memory neural networks (LSTMs) (Dikshit et al., 2021a)). These algorithms can be used to simulate
90 the evolution of future droughts and construct risk maps for drought contingency planning (Rahmati et al.,
91 2020). Among the different models, the LSTMs can effectively simulate short-term and long-term streamflow
92 series, and their performances have been validated at short temporal scales (Dikshit et al., 2021b; Kang et al.,
93 2023).

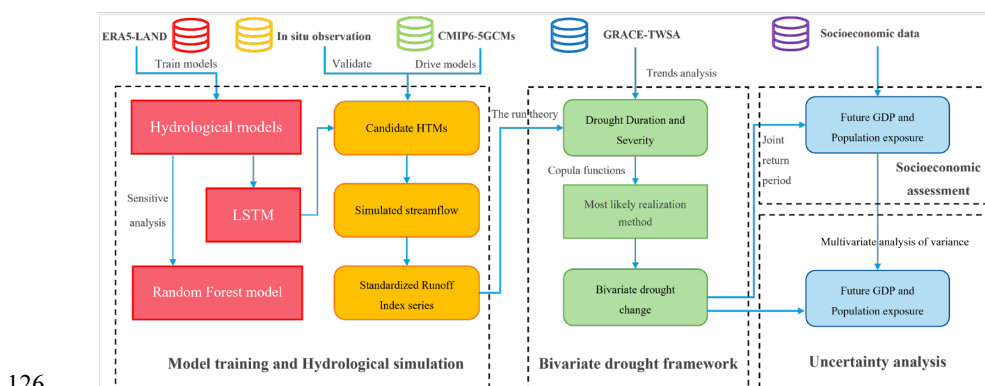
94 In this study, we project changes in bivariate hydrological drought characteristics (duration and severity)
95 and their associated socioeconomic risks under three SSPs (i.e., SSP1-26, SSP3-70, and SSP5-85) over 179
96 catchments in China. To achieve this, we combine five hydrological models and a deep learning model (i.e.,
97 the LSTM), and then drive the hybrid model with the five bias-corrected GCMs outputs under Coupled Model
98 Intercomparison Project phase six (CMIP6). Then, we employ a machine learning-based framework (i.e.,
99 Random Forest, RF model) to quantify the sensitivity of different meteorological variables to daily
100 streamflow. We employ the run theory and two drought metrics, the SRI and TWS-DSI, to identify and
101 explore recent changes in drought characteristics. In addition, we use Copula functions to build the bivariate
102 model of drought duration and severity during both reference and future periods. After identifying shifts in
103 bivariate drought characteristics based on the most likely realization approach, we project the exposure of
104 gross domestic product (GDP) and population to increasing drought risks in the future. Finally, we decompose
105 the uncertainties arising from different sources by employing the multivariate analysis of variance
106 (MANOVA) method. The paper provides a clear description of materials and methods used to analyze, and
107 then shows the difference between two drought indexes to assess drought conditions, the contribution of
108 meteorological factors to simulate streamflow, the validation of the accuracy of HTMs, the evolution of



109 univariate and bivariate droughts in future scenarios and the socioeconomic exposure to bivariate droughts.
 110 We also make a discussion of uncertainty from multisource data and cascade model chain, and reflect on
 111 limitations that could be improved to enhance the further study. All findings are summarized and targeted to
 112 propose drought mitigation strategies.

113 2. Methodology

114 The workflow of this study is divided into four modules (Figure 1), described briefly below and detailed
 115 in the following sections. In step 1, the hydrological models and LSTM are trained using the ERA5-Land
 116 dataset, then the output of HMs is used as input to feed the LSTM, thus we build the hybrid terrestrial models
 117 (HTMs). In step 2, the trained HTMs are validated using in situ streamflow observations, then driven by
 118 using the outputs of five GCMs from the CMIP6 to project streamflow and the SRI series. In step 3, monthly
 119 drought characteristics (i.e., drought duration and severity) are defined using run theory and combined with
 120 Copula functions to construct a bivariate drought framework. Future bivariate drought change is evaluated
 121 using the most likely realization method. Meanwhile, the TWS measurements from GRACE missions are
 122 also employed to characterize recent changes in TWS-based droughts, which are also compared with the
 123 hydrological droughts. In step 4, we employ future scenarios of GDP and population alongside our future
 124 drought projections to produce a socioeconomic assessment of drought exposure over China. Finally, we
 125 examine the contribution of uncertainty from different sources in projecting drought change and exposure.



126
 127 **Figure 1. Schematic flowchart of the method, including ML-constrained hydrological simulations, evaluation of**
 128 **bivariate hydrologic drought characteristics and change, and the socioeconomic evaluation to drought exposure**
 129 **under climate change.**

130 2.1 Derivation of 2-meter relative and specific humidity

131 The Clausius–Clapeyron relationship is used to derive saturated vapor pressure (e_s) and air temperature
 132 (T), and is expressed as follows (Koutsoyiannis, 2012):



133
$$e_s(T) = e_0 \exp \left[\left(\frac{1}{T_0} - \frac{1}{T} \right) \frac{L_0}{R_0} \right] \quad (1)$$

134 where T_0 , e_0 , L_0 and R_0 are constants, with a value of 273.16 K, 611 Pa, 2.5×10^6 J kg⁻¹, 461 J kg⁻¹ K⁻¹,
135 respectively;

136 Since near-surface relative humidity (RH) can't be directly obtained from the ERA5-Land dataset, the
137 2m temperature (T_{2m}) and dew-point temperature (T_d) are substituted into equation (1) to calculate RH :

138
$$RH = \frac{e_s(T_d)}{e_s(T_{2m})} = \exp \left[\left(\frac{1}{T_{2m}} - \frac{1}{T_d} \right) \frac{L_0}{R_0} \right] \quad (2)$$

139 Then, the near-surface air pressure (ps) and T_d are used to deduce the specific humidity (SH), which is
140 mathematically expressed as follows (Simmons et al., 1999):

141
$$SH = \frac{0.622 \times e_s(T_d)}{ps - 0.378 e_s(T_d)} \quad (3)$$

142 2.2 Sensitivity analysis on meteorological variables for runoff

143 The RF model is used to calculate the sensitivity to different meteorological variables for runoff,
144 including precipitation (pr), air pressure (ps), surface downwelling shortwave and longwave radiation ($srsds$
145 and $srlsds$), RH , SH , average temperature, maximum and minimum temperature. The contribution of a key
146 variable is derived by using the pre-established model, the perturbed meteorological variable and remaining
147 (non-perturbed) variables (Antoniadis et al., 2021; Green et al., 2020). The percentage change in streamflow
148 is derived from the following equation:

149
$$S_i = \frac{\text{mean}(R_{(i+1SD)} - R_{(all)})}{\text{stdev}(R_{obs})} \times 100\% \quad (4)$$

150 where S_i indicates the sensitivity of streamflow to i^{th} meteorological variable, which are pr , ps , SH , RH , $srlsds$,
151 $srsds$ and temperature; R_{obs} is the observation of streamflow which has units of m³/s; $R_{(i+1SD)}$ is the simulated
152 streamflow by perturbing i by +1 SD; $R_{(all)}$ is the streamflow simulated by all meteorological variables; stdev
153 (R_{obs}) represents the standard deviation of R_{obs} .

154 2.3 Deep learning-constrained hydrological modeling

155 2.3.1 Conceptual hydrological models

156 For preliminary hydrological simulations, we select five hydrological models to represent hydrological
157 characteristics under different environments. The GR4J (Génie Rural à 4 paramètres Journalier) is a lumped
158 model with 4 parameters developed by Perrin et al. (2003). GR4J consists of two water store modules (runoff
159 yielding and routing) and uses daily rainfall and evapotranspiration as inputs to simulate streamflow series



160 (Kunnath-Poovakka and Eldho, 2019). This model has been successfully used to simulate hybrid runoff
161 processes in many continents (Shin and Kim, 2021; Gu et al., 2023). Additionally, we use the temperature-
162 based method (Oudin et al., 2005) to estimate the potential evapotranspiration of the GR4J model.

163 The HBV (Hydrologiska Byråns Vattenbalansavdelning) model was initially developed by the Swedish
164 Meteorological and Hydrological Institute for hydrological forecasting (BERGSTRÖM and FORSMAN,
165 1973). This model including five modules and one transform function to quantify hydrological variables (i.e.,
166 precipitation, snow, soil moisture, runoff, baseflow) (Bergström, 1995). It has been widely employed to
167 simulate streamflow, and it particularly has good capacity in simulating snowmelt runoff (Kriauciuniene et
168 al., 2013).

169 The HMETs (hydrological model of École de technologie supérieure) model contains 21 parameters
170 and two reservoirs (i.e., the saturated and vadose zones), which makes it simplified and efficient to complete
171 hydrological simulation (Martel et al., 2017). The model can simulate six processes in water cycle, including
172 the accumulation, melt and refreezing of snow, water infiltration and routing, evapotranspiration (Qi et al.,
173 2020). It has been growly used for streamflow simulation under climate change and has shown well
174 performance (Chen et al., 2018).

175 The SIMHYD (simple lumped conceptual daily rainfall-runoff) model is a daily rainfall-runoff model
176 developed by Porter and McMahon (1975). There are four types of runoff from different sources: impervious
177 areas, infiltration, interflow, and groundwater store (Chiew et al., 2002). Although the model was developed
178 earlier, it has shown good accuracy in simulating runoff over China (Yu and Zhu, 2015).

179 The XAJ (Xinanjiang) model is a hydrological model, which can usually achieves better performance
180 in humid and semi-humid areas than in arid areas (Zhao, 1992). It is composed of a three-layer
181 evapotranspiration module with four parameters and separates the runoff into four components (i.e., surface
182 water, groundwater, interflow water and flow routing) (Tian et al., 2013). To date, it is widely reported that
183 the XAJ model usually show the best accuracy in simulating hydrological conditions in China (Hu et al.,
184 2005).

185 We use the SCE-UA (Shuffled Complex Evolution) approach with maximizing the objective function
186 (i.e., Kling-Gupta efficiency) to optimize these models (Duan et al., 1992). The most complete 20-year
187 observation period is selected to calibrate the models in each watershed. To calibrate the hydrological models,
188 a cross-validation method developed by Arsenault et al. (2017) is used, which employs the odd years of data
189 to calibrate models, and the even years of data to validate.

190 2.3.2 Hybrid scheme of hydrological model and machine learning

191 Recurrent neural network (RNN) models have had considerable success in hydrological modeling (Cho
192 et al., 2014; Sherstinsky, 2020). However, when considering long input sequences, RNNs struggle to capture
193 the relationships between distant points due to a phenomenon known as “long-term dependencies” (Yu et al.,
194 2019). With the development of deep learning, this problem can be successfully avoided by using LSTMs.

195 A LSTM cell includes input, output and forget gates. The input gate determines which new information



196 can be stored in the cell state, and the forget gate identifies which information will be discarded from the cell
197 state. The output gate controls what part of the cell state is selected as the output. The updated cell state is a
198 combination of the information retained and the new information to be added. By using this architecture, the
199 LSTM can avoid the problem of gradient vanishing or explosion during backpropagation, especially when a
200 series is long (Gers et al., 2000). The LSTM can be expressed as follows:

$$201 \quad fg_t = \sigma(W_{hf}hs_{t-1} + W_{xf}x_t + b_f) \quad (5)$$

$$202 \quad ig_t = \sigma(W_{hi}hs_{t-1} + W_{xi}x_t + b_{fg}) \quad (6)$$

$$203 \quad \tilde{c}_t = \tanh(W_{hc}hs_{t-1} + W_{xc}x_t + b_c) \quad (7)$$

$$204 \quad c_t = fg_t \cdot c_{t-1} + ig_t \cdot \tilde{c}_t \quad (8)$$

$$205 \quad og_t = \sigma(W_{oh}hs_{t-1} + W_{ox}x_t + b_o) \quad (9)$$

$$206 \quad hs_t = og_t \odot \tanh(c_t) \quad (10)$$

207 where x_t , fg_t , ig_t and og_t are input variables, and forget, input and output gates at time t , respectively; W_i ,
208 W_e , W_f and W_o are the weights of each gate; the operator ‘ \odot ’ is the symbol for the dot product of two vectors;
209 c_t and hs_t are the cell state of the LSTM and the hidden unit at the time t , c_{t-1} and hs_{t-1} at the former time
210 $t - 1$; \tilde{c}_t is the activation function of hidden layer; b_i , b_f , b_o and b_c are bias items and the; $\sigma(\cdot)$ and $\tanh(\cdot)$
211 are the sigmoid function and the hyperbolic tangent function, respectively; at the initial moment, cell and
212 hidden states are set to zero arrays.

213 The hydrological outputs together with other climate variables are used as inputs to feed the LSTM
214 model (i.e., the HTMs are thus constrained by the LSTM). Because changes in meteorological variables require
215 some time to converge before they are reflected in the runoff, it is essential to calculate the lag time caused
216 by the flow convergence for the model. The catchment response lag time d is defined as the time during
217 which precipitation accumulates in the river to generate runoff for the gauge downstream, and is
218 mathematically expressed as follows (Berne et al., 2004; Ganguli and Merz, 2019):

$$219 \quad d = 2.51A_d^{0.4} [\text{hrs}] = 0.11A_d^{0.4} [\text{days}] \quad (11)$$

220 where A_d (km^2) represents the catchment area; meteorological variables from day $T-d$ to day T are employed
221 to drive HTMs.

222 We combine the five hydrological models with LSTM to construct five HTMs. To compare the
223 performance of the HTMs, we use ten HTMs as candidates for streamflow simulation in each catchment. The
224 calibrated HTMs are then driven by the outputs of five GCMs under each SSP (aggregated to produce a basin
225 average series) during 1985-2100 over 179 catchments to project future daily streamflow.



226 2.4 Drought indexes and run theory

227 The TWS-DSI is employed to measure the degree of terrestrial drought severity (Zhao et al., 2017). It
228 is a dimensionless standardized water storage anomaly index, which can indicate terrestrial drought
229 conditions when below the mean standard value. The TWS-DSI can be mathematically expressed as follows:

$$230 \quad TWS-DSI_{x,y} = (TWS_{x,y} - \overline{TWS}_y) / \sigma_y \quad (12)$$

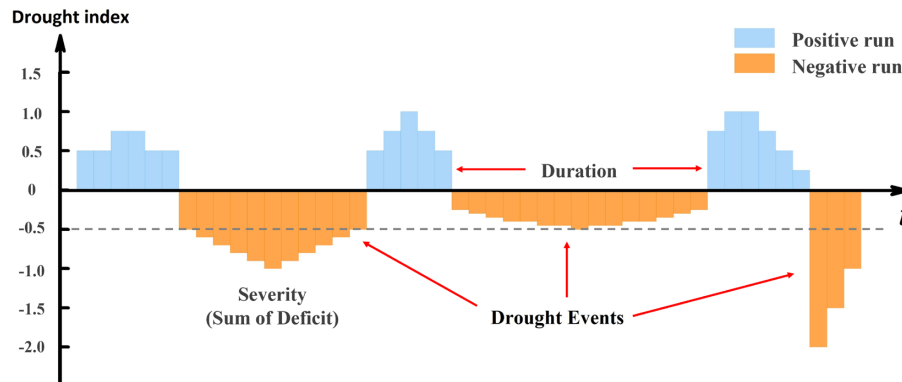
231 where $TWS_{x,y}$ is the TWS at year x and month y ; \overline{TWS}_y and σ_y represent the means and standard deviation
232 of TWS at month y , respectively.

233 The SRI is a measure of the variability of runoff for a given duration based on the percentage of
234 accumulated runoff. (Shukla and Wood, 2008). To calculate the SRI, we simulate the retrospective time series
235 of streamflow and fit the sample series to a probability distribution. The SRI is considered to follow a Pearson
236 type-III distribution (Vicente-Serrano et al., 2012), and is calculated as follows:

$$237 \quad SRI = \begin{cases} -\left(r - \frac{c_0 + c_1 r + c_2 r^2}{1 + d_1 r + d_2 r^2 + d_3 r^3}\right) & 0 < F(x) \leq 0.5 \\ r - \frac{c_0 + c_1 r + c_2 r^2}{1 + d_1 r + d_2 r^2 + d_3 r^3} & 0.5 < F(x) \leq 1 \end{cases} \quad (13)$$

238 where $r = \sqrt{\ln \left[\frac{1}{F(x)^2} \right]}$; $F(x)$ is the cumulative probability density of SRI; c_0 , c_1 , c_2 , d_1 , d_2 and d_3 are
239 the empirical constants, taken as 2.516, 0.803, 0.010, 1.433, 0.189, 0.001, separately.

240 After calculating the two drought indexes, the degree of water deficit can be determined according to
241 the Grades of Meteorological Drought and the previous classification (Dikici, 2020). [Table S1](#) presents the
242 drought classification and thresholds used for identifying drought degrees. The run theory is employed to
243 obtain characteristics of drought events from the time series (Yevjevich, 1967). When the drought index is
244 below the mild drought (i.e., ≤ -0.5 drought index), a drought event is detected ([Figure 2](#)), and then the drought
245 duration and drought severity are extracted.



246

247

248

Figure 2. Drought duration and severity identification based on run theory, where -0.5 denotes the drought threshold (grey dash line).

249

2.5 Socioeconomic exposure assessments based on the Copulas and most likely realization

250

After extracting the drought duration (D) and severity (S), we fit their marginal distributions with seven distributions shown in Table S2. The OR case (i.e., a bivariate drought event is identified with either a high severity or long duration) of the joint return period (JRP) under a Copula-based framework is used to quantify the occurrence of drought events (Yin et al., 2020). The joint distribution of drought duration and severity is constructed by using a Copula function, which is valuable for describing correlated hydrological variables (Li, 1999). Unlike univariate drought frequency analysis, the JRP within a bivariate framework can be represented by an isoline, which contains infinite combinations of multivariate variables. It is important for risk assessments to select a representative combination along the isoline. Previous studies have typically selected joint design values according to the same frequency hypothesis, but this approach lacks a statistical basis and poorly describes the physical characteristics of droughts (Yin et al., 2018). In this paper, the joint probability density is used to optimize the most likely realization, which is mathematically expressed as follows:

261

262

$$\begin{cases} (d^*, s^*) = \arg \max f(d, s) = c[F_d, F_s] \cdot f_d \cdot f_s \\ C[F_d, F_s] = 1 - \mu / T_{or} \\ c[F_d, F_s] = \frac{dC(F_d, F_s)}{d(F_d)d(F_s)} \end{cases} \quad (14)$$

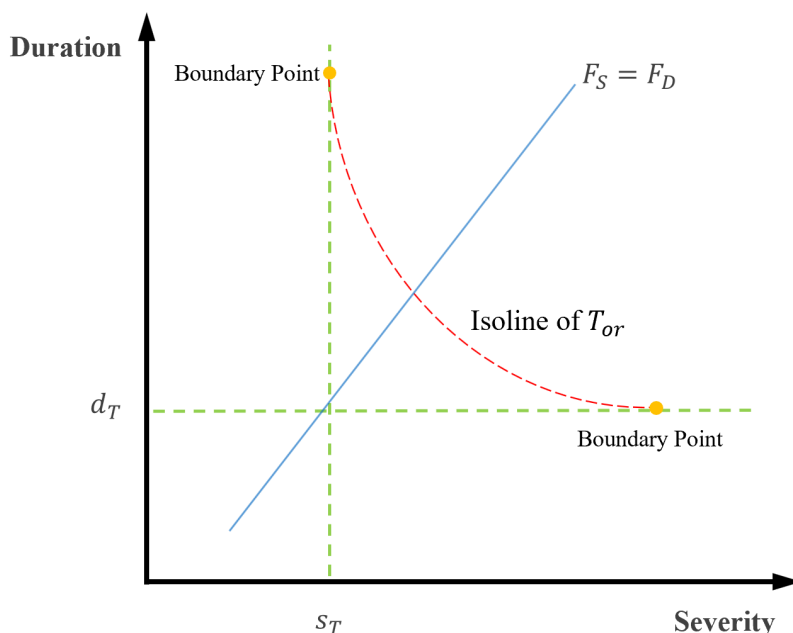
263

where $c[F_d, F_s]$ is the Copula probability density function; f_d and f_s are the fitted probability density functions of D and S , respectively; F_d and F_s are the marginal distribution of D and S , respectively; (d^*, s^*) is the most likely realization under a given JRP T_{or} ; μ is the mean inter-arrival time between two consecutive droughts.

264

265

266



267
 268 **Figure 3. Joint distribution of drought duration and severity under a critical T_{or} . The green lines are two arbitrary**
 269 **values of duration and severity. The red line is the isoline line of two variables under a critical T_{or} , and the blue**
 270 **line denoted the traditional equal-frequency assumption.**

271

272 Socioeconomic exposure has previously been defined as ranging from 0 to 100% in the future period
 273 (Gu et al., 2020a), but dynamically shifting climate risks cannot be represented under this static definition.
 274 Here, the socioeconomic exposure is defined by considering the shift in JRP, and is expressed at the catchment
 275 scale as follows:

276
$$E_{POP} = \frac{T_h I(T_h - T_f)}{T_f A_d} \times POP \quad (15)$$

277
$$E_{GDP} = \frac{T_h I(T_h - T_f)}{T_f A_d} \times GDP \quad (16)$$

278 where E_{POP} and E_{GDP} denote the population and GDP exposure; T_h and T_f denote the historical and
 279 future JRP, respectively; $I(\cdot)$ denotes the controlling function, which is 1 when $T_h - T_f > 0$, or 0 when
 280 $T_h - T_f \geq 0$ is recorded; POP (GDP) denotes the population (GDP) of a given catchment in the future
 281 climate.



282 2.6 Quantifying the uncertainty contributed by different sources

283 Uncertainties in the future drought projections can arise from the SSPs, GCMs and HTMs. During both
284 historical (1985-2014) and future periods (2071-2100), the combination of 3 SSPs, 5 GCMs and 5 HTMs
285 through the impact modeling chain resulted in 150 hybrid combinations. The overall uncertainty is calculated
286 from the variance of the future estimated JRP relative to the historical 50-year droughts. To partition the
287 uncertainty from different sources of data and their interactions effects, the MANOVA is used and expressed
288 as follows (Weinfurt, 1995):

$$289 \Delta y_{x,y,z} = M + S_x + G_y + H_z + I_{x,y,z} \quad (17)$$

290 where M denotes the mean change of all indicator in models; S_x , G_y and H_z denote the impact on
291 indicators of the x^{th} SSP, y^{th} GCM and z^{th} HTM, respectively; $I_{i,j,k}$ is the overall impact arising from the
292 interactions of different sources. And the overall variance V is then expressed as follows:

$$293 V = VS + VG + VH + VI_{SG} + VI_{SH} + VI_{GH} + VI_{SGH} \quad (18)$$

294 where VS , VG , VH are the variance from the SSPs, GCMs and HTMs, respectively. VI_{SG} , VI_{SH} , VI_{GH}
295 and VI_{SGH} denote the variance caused by the coupling between different sources of data. The contribution
296 of each source to the overall uncertainty is quantified by the variance of each source by the total variance.

297 3. Data and materials

298 3.1 In situ observation dataset

299 We use a gridded meteorological dataset with $0.5^\circ \times 0.5^\circ$ resolution, including daily temperature
300 (maximum, minimum and average, °C) and daily precipitation (mm) from 1961 to 2018, provided by the
301 National Meteorological Bureau of China. The dataset is regarded as the latest gridded meteorological dataset
302 in China and has been applied to some studies (e.g., Wu et al., 2018; Yin et al., 2021a,b). Meanwhile, we
303 gathered the daily streamflow of 463 in situ hydrological stations spanning different periods during 1961-
304 2018. The hydrological stations are densely distributed in East China, while West China has a sparser
305 distribution. Through rigorous data quality checks, 179 unnested basins with at least 20 years of data are
306 selected, covering nine major watersheds in China. For more details on streamflow data processing and
307 catchment screening, please refer to Yin et al. (2021b).

308 3.2 GRACE/GRACE-FO measurements

309 Temporal variations in the Earth's gravitational field observed by GRACE satellites have been used to
310 retrieve TWS data (Tapley et al., 2004). Many international institutes have released the TWS mascon products
311 at a monthly scale, including the JPL (Jet Propulsion Laboratory of the California Institute of Technology),



312 the GSFC (Goddard Space Flight Center of NASA), and the CSR (Center for Space Research of the
313 University of Texas). As these three mason solutions are produced different spatial resolutions, we produce
314 a blended TWS data based on the average of JPL, GSFC and CSR with $0.5^{\circ} \times 0.5^{\circ}$ resolution from 2002 to
315 2022, and fill the missing data using a linear interpolation approach (Yin et al., 2022).

316 **3.3 ERA5-Land dataset**

317 ERA5-Land is a dataset that consists of a large volume of meteorological variables, including
318 precipitation, temperature and air pressure etc. The spatial resolution of dataset is 9 km and the temporal
319 resolution is one hour (Yilmaz, 2023). Under the latest global reanalysis and the lapse rate correction, the
320 ERA5-Land reanalysis dataset provides a substitute for unavailable observed weather data, by taking the
321 effect of altitude on the spatial scheme of climate variables into consideration (Pelosi et al., 2020). Six
322 variables are used in the study (i.e., *pr*, *ps*, T_{2m} , T_{dew} , *srlsds*, *srsds*) and aggregated to a daily scale from the
323 hourly scale before conducting data analysis.

324 **3.4 Bias-corrected GCM outputs and socioeconomic scenarios**

325 The climate outputs of five GCMs under historical scenario and three SSPs (i.e., SSP1-26, SSP3-70,
326 SSP5-85) under CMIP6 are used to represent climate scenarios. The series of bias-corrected variables have
327 been downscaled to $0.5^{\circ} \times 0.5^{\circ}$ resolution from 1850 to 2100 under the Intersectoral Impact Model
328 Intercomparison Project 3b (ISIMIP3b) (Lange, 2019). To reduce the systematical biases of CMIP6 raw
329 outputs, seven variables from the bias-corrected ISMIP3b dataset have been used, namely temperature (daily
330 average, maximum and minimum), *pr*, *ps*, *srsds*, *srlsds*, *RH* and *SH*.

331 Population and GDP data under three SSPs are employed to evaluate the potential socioeconomic risks
332 of drought in a warming world. An open-access population dataset is adopted which takes into consideration
333 the universal two-child policy, the census results and the statistical annual report (Jiang et al., 2017). The
334 economic index from 2010 to 2100 is estimated based on the Cobb-Douglas and Population-Environment-
335 Development model (Jiang et al., 2018). All of the data have been previously used to assess the socio-
336 economic impact of extreme hydrologic hazards (Yin et al., 2022; Yin et al., 2023).

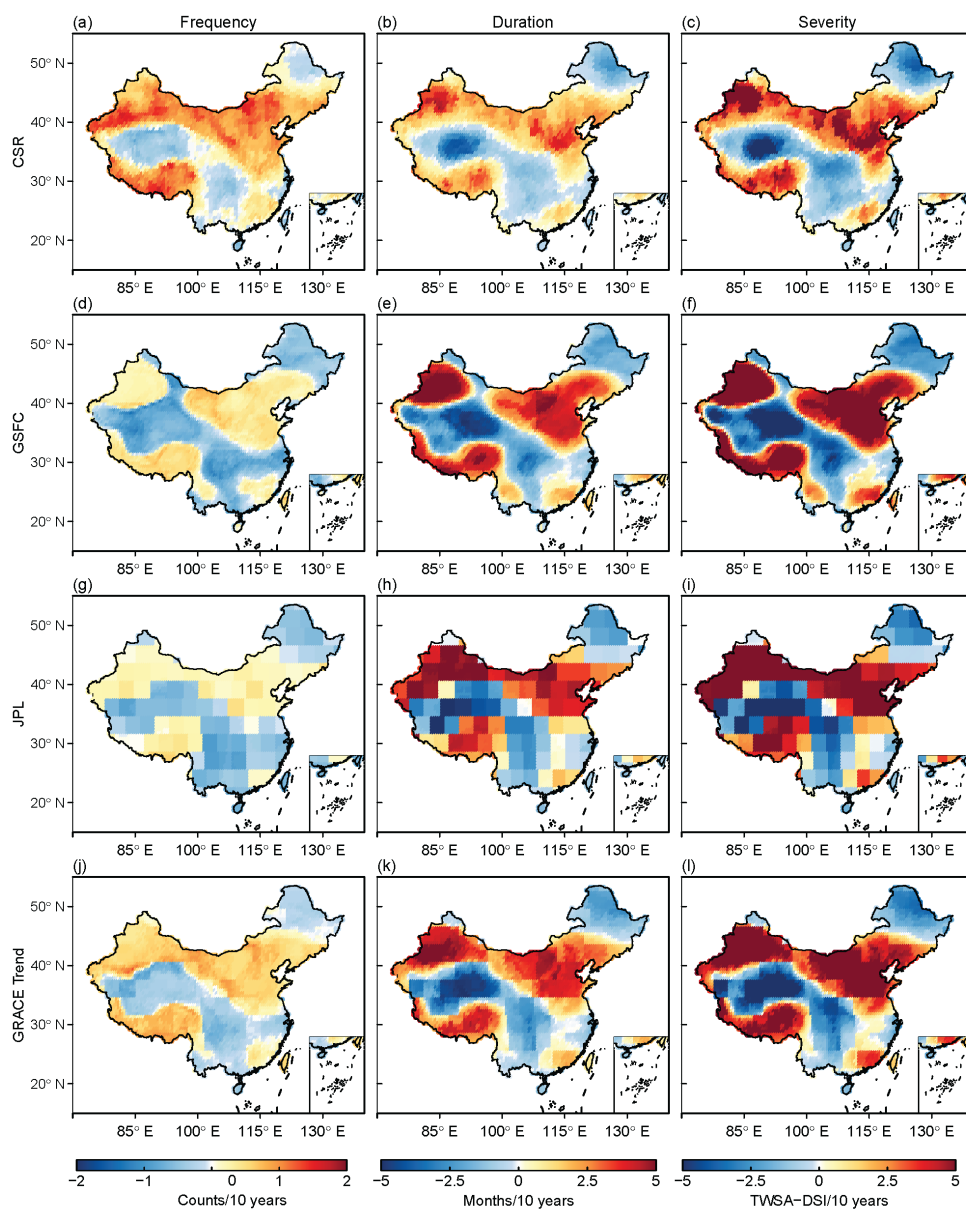
337 **4. Results**

338 **4.1 Observed changes in SRI and TWS based drought**

339 As there are insufficient streamflow observations to compute the SRI in northwest China, we also
340 employ the TWS-DSI as a supplement. This approach enriches the variety of water storage or flux being
341 evaluated. Trends in drought characteristics (i.e., frequency, duration and severity) are estimated by using the
342 GRACE/GRACE-FO dataset and observed runoff across China. [Figure 4](#) and [Figure 5](#) show the drought
343 trends based on the TWS-DSI and SRI, respectively. Overall, the two indexes show similar trends in most
344 catchments, suggesting that drought hazards have increased in recent decades. TWS-DSI droughts have

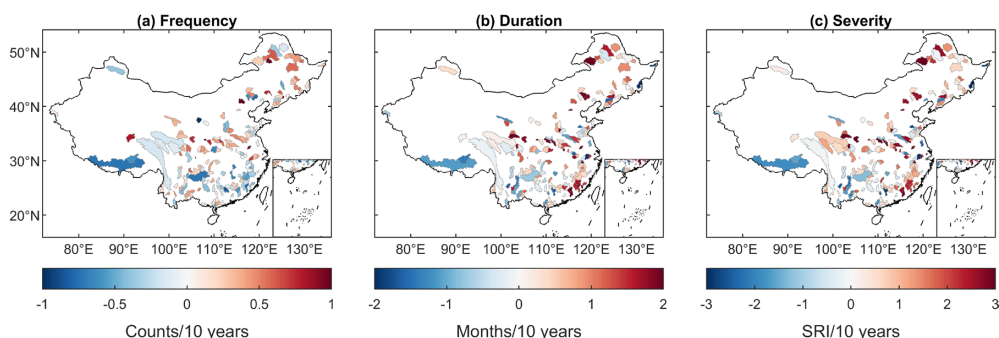


345 increased in 54% of areas, which are mainly located in the Qinghai-Tibet Plateau, the North China Plain and
346 the northwestern Xinjiang Province. Likewise, SRI droughts have increased over 51% of studied catchments,
347 which mainly dominates northeastern and southeastern China. The severity of droughts measured by the
348 TWS-DSI index is twice of the hydrological drought, primarily because the TWS-DSI metric incorporates
349 all vertical water fluxes, offering a comprehensive view of shifts in water scarcity. Some locations exhibit
350 discrepancies depending on the index considered. For instance, droughts in the Qinghai-Tibet Plateau and
351 Northeast China show opposite trends. Anomalies in the Qinghai-Tibetan plateau may be explained by the
352 transformation of snowpack melt into surface runoff under the influence of climate change, which helps
353 compensate for the lack of surface water in the area (Stewart, 2009). The discrepancy observed in
354 Northeastern China could potentially be linked to the rise in soil moisture from increased infiltration, which
355 causes a higher proportion of water to be stored within the soil than at the surface, interfering with the
356 quantification of hydrological drought (Wang et al., 2017). Finally, both indicators show a consistent positive
357 drought trend in most areas of China and particularly the North China Plain and Pearl River Basin.



358
 359
 360

Figure 4. Trends in drought frequency, duration and severity based on the TWS-DSI from 2002 to 2022 using three GRACE/GRACE-FO products (a-i) and the blended data (j-l).

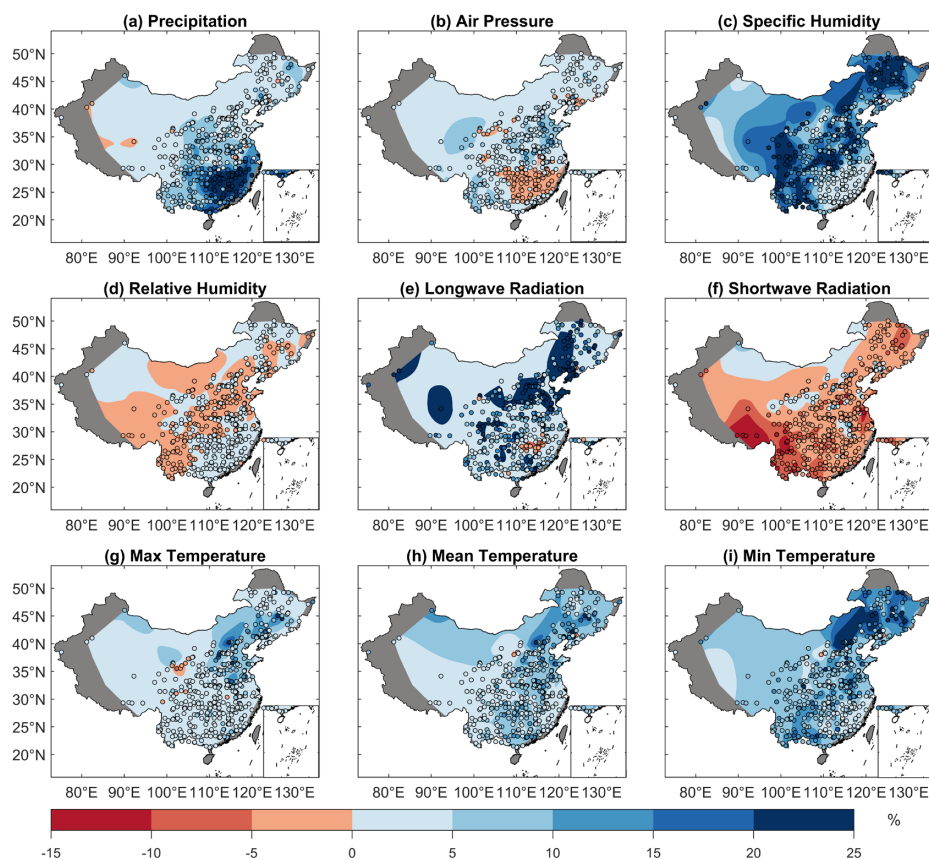


361

362 **Figure 5. Trends in drought frequency, duration and severity based on SRI over China.**

363 **4.2 Machine Learning-constrained streamflow simulation and model evaluation**

364 The RF model is used to quantify the sensitivity of streamflow to different meteorological variables
365 (Figure 6). Precipitation typically plays a major role in generating runoff in Southeast China, although *SH*
366 plays the most important role in some regions such as Central, Southwest and Northeast China. Over 30%
367 and 38% of stations show a sensitivity rate of >10% in Western and Northeastern China, respectively. In
368 contrast, *RH* and shortwave radiation have a negative contribution to streamflow; especially shortwave
369 radiation, which has a pronounced negative sensitivity in 394 stations probably due to enhanced
370 evapotranspiration (Ma et al., 2019). In general, *RH* contributes to increasing streamflow over most regions
371 of China, but the opposite effect is observed in 179 stations mainly located in Southwestern China, Yellow
372 River and Huaihe River basins. This is the result of the mutual feedback of water and heat dynamics (i.e.,
373 saturated vapor pressure increases with warming and intensifies evaporation, leading to a decrease in surface
374 water), which was also found by Liu et al. (2017). The temperature has a positive contribution in Northeast
375 China, suggesting that runoff in this region is likely to increase in the context of climate warming, leading to
376 a reduction in drought over the regions.



377

378

379

Figure 6. Sensitivity of meteorological variables to daily streamflow. The figure uses a thin plate smoothing spline method to interpolate the point-based station data (circles). Gray areas indicate missing data.

380

381

382

383

384

385

386

387

388

389

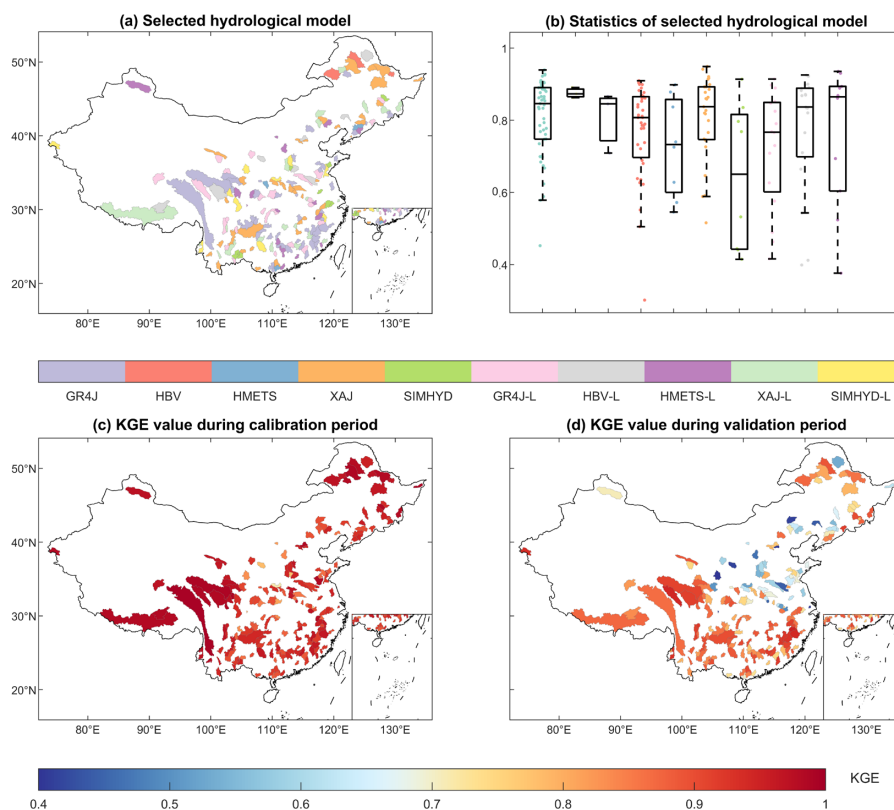
390

391

392

393

The performances of simulated streamflow by different HTMs are shown in Figure 7. The model that has the largest KGE is considered to be the best-performing in each catchment. In Fig 7. (a) and (b), the GR4J and GR4J-LSTM performed best in 77 out of 179 studied catchments. The median KGE value of GR4J is higher than 0.83, revealing a superior performance than the other hydrological models. Subsequently, the XAJ and XAJ-LSTM are the best models in 57 catchments, mainly located in the southern Yangtze River. Last, the HBV and HBV-LSTM performed best in only 10 catchments, where the streamflow are impacted by snowfall in plateaus and northern frozen areas. All catchments exhibit KGE values greater than 0.9 during the calibration period in Figure 7c, showing good performance in simulation. During the validation period, only 18 catchments have KGE values below 0.6, and most of the catchments have KGE values greater than 0.8 in Figure 7d. In summary, the trained models simulate streamflow well in all the studied catchments. Additionally, the KGE values in the southern region are generally higher than those in the northern region during the validation period, which is consistent with previous hydrological simulation works (Gu et al., 2020b, 2021). This phenomenon may be attributed to the higher dependence of streamflow on rainfall in South China, which is governed by a humid climate pattern (Zheng et al., 2022).



394

395 **Figure 7. Hydrological simulation performances of all candidate models. (a), The best-performing model with the**
396 **highest KGE value. (b), Boxplots of all catchments for ten HTMs indicated by KGE values. (c)-(d), The highest**
397 **KGE values during the calibration (c) and validation (d) period, respectively.**

398

4.3 Projected changes in univariate drought characteristics

399

We project the future daily runoff series by driving the HTMs with the bias-corrected CMIP6 variables, and then we estimate the monthly SRI to identify drought duration and severity. Based on the maximum Bayesian Information Criterion (BIC), we select the best-performing marginal distributions for duration and severity from seven candidate distributions, based on historical data for each catchment. Figure 8 and Figure 9 show the multi-model ensemble average severity and duration for the 50-year historical return period (RP).

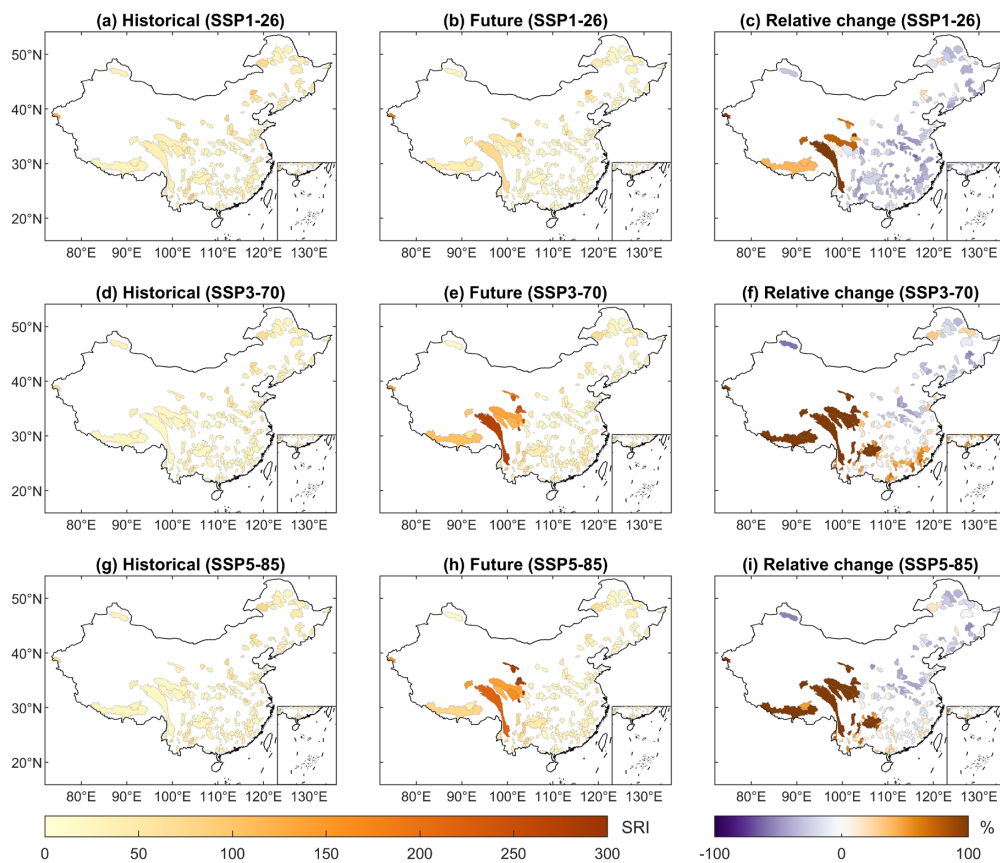
404

In western China, we project a significantly increasing drought trend under the three SSPs, which indicates potential for increased water scarcity and more frequent extreme drought events. In Southeast China, we project that droughts are likely to intensify under SSP3-70 but not under SSP5-85. It is generally considered that SSP5-85 is accompanied by higher carbon emissions than that of SSP3-70 (O'Neill et al., 2016). However, future works also take significant action to control the extent of climate change combined with strong climate policies under SSP5-85 (Fujimori et al., 2017). As a result, there is no deterioration of drought severity with policy interventions, which emphasizes the significance of ensuring the implementation

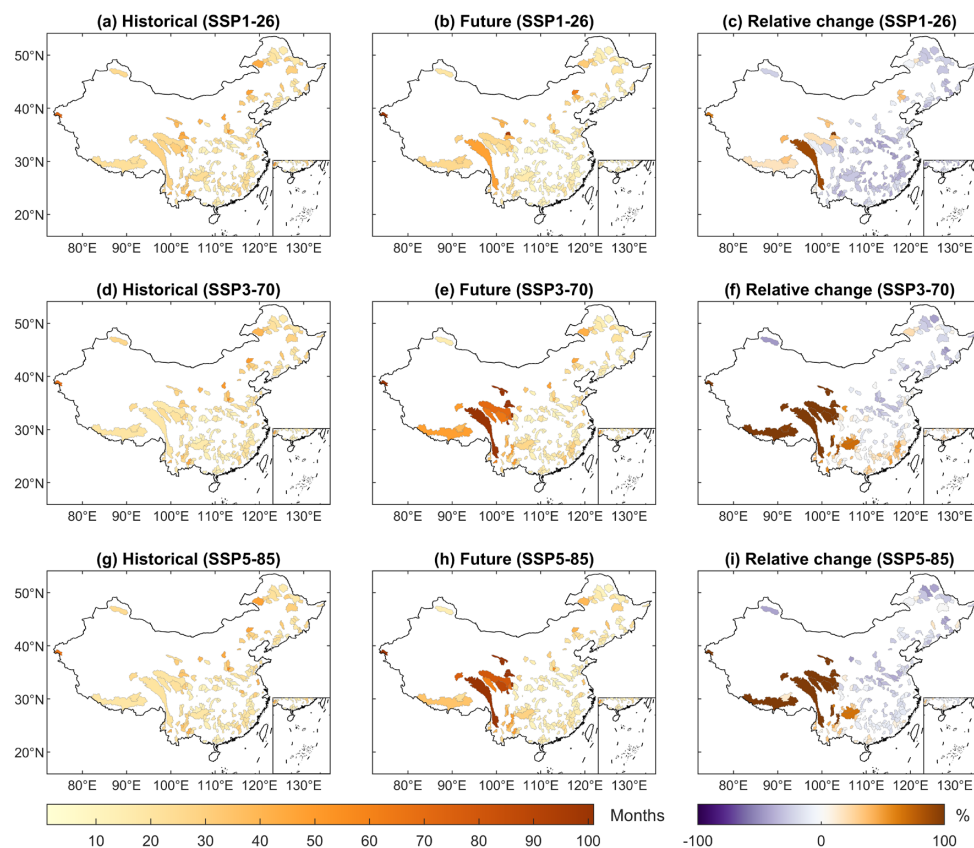
410



411 of climate strategies. In northern China, in contrast, we find that future drought risks are projected to decrease
412 under the three scenarios, which is possibly related to more moisture convergence from the East Asian
413 monsoon circulation as the warming climate (Chowdary et al., 2019).

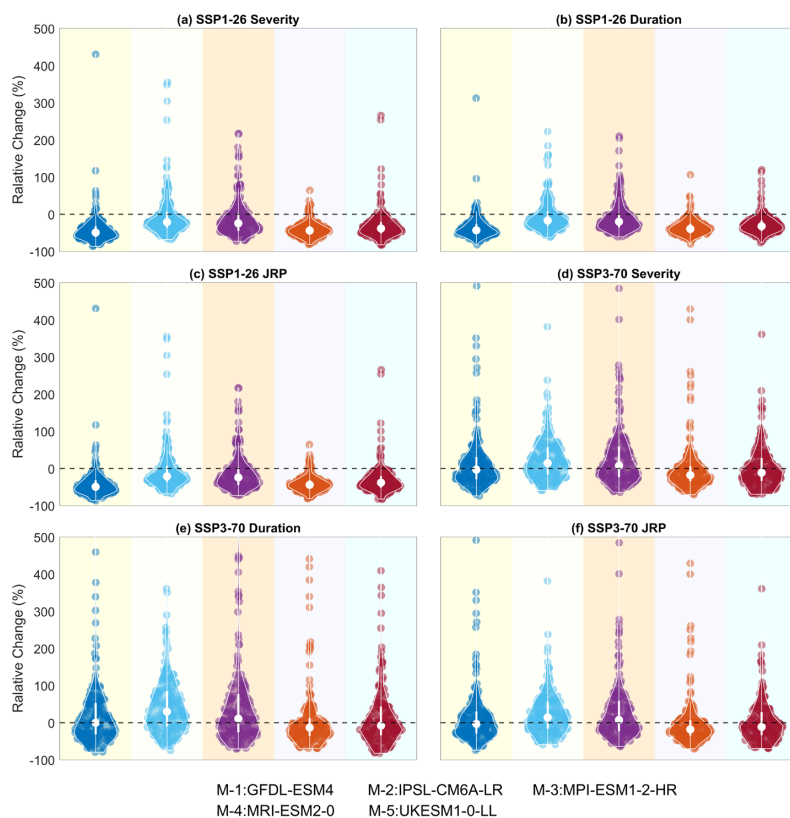


414
415 **Figure 8.** Multi-model ensemble average design severity (dimensionless) under a 50-year RP for three SSPs, and
416 relative changes (%) in 2071-2100 compared to 1985-2014.



417
418 **Figure 9. Multi-model ensemble average design duration (months) of the multi-model for a 50-year RP for three**
419 **SSPs, and relative changes (%) in 2071-2100 compared to 1985-2014.**

420 We display the relative change of drought characteristics under 50-year RP for all catchments for five
421 GCMs under the three SSPs using violin plots (Figure 10). For most catchments, the relative change of
422 drought duration and severity is negative. However, the relative change under some scenarios reached a
423 maximum of 400%, highlighting the extreme change of drought. The median relative change of severity
424 based on the IPSL_CM6A_LR under SSP3-70 are 30%, and 22% of catchments have a relative change over
425 200%, representing the most severe case of drought evolution. Furthermore, the distributions of the
426 projections based on the MPI-ESM1-2-HR, MRI-ESM2-0 and UKESM1-0-LL models are highly skewed
427 and bimodal under SSP3-70 and SSP5-85, revealing substantial spatial heterogeneity across China. Overall,
428 the severity and duration of droughts slight increase in some catchments and have the risk of extreme
429 intensification as global warming.



430

431 **Figure 10. Violin plots of relative changes (%) in severity and duration to the historical drought event with 50-**
432 **year RP under three SSPs. The white circles are the median values of relative changes.**

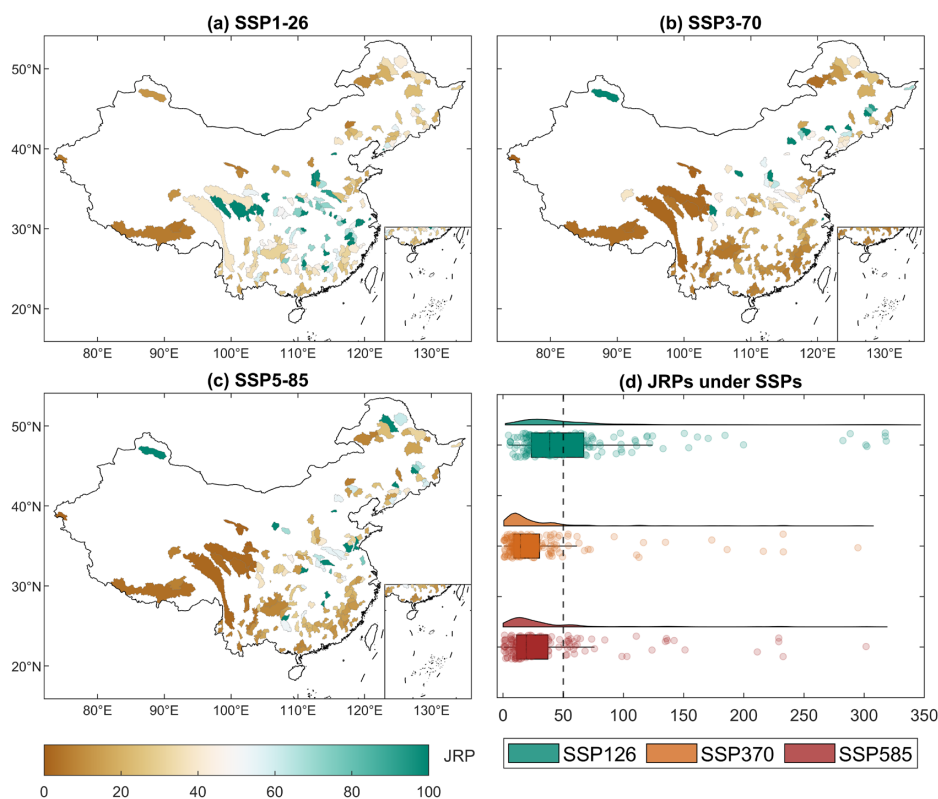
433 4.4 Bivariate drought changes and corresponding socioeconomic risks

434 To capture the complex dependence structure between drought severity and duration, we use a Copula
435 function to quantify the bivariate risk of hydrological droughts under climate change. Changes in the JRP of
436 the historical (1985-2014) drought event with 50-year JRP in the future (2071-2100) period are shown in
437 [Figure 11](#). The medians of the projected future JRP are 38.78, 14.52 and 19.24 under SSP1-26, SSP3-70 and
438 SSP5-85, respectively. For 69% and 60% catchments under SSP3-70 and SSP5-85, we find the JRP of the
439 50-year drought is reduced to less than 25 years in the future period, suggesting that the risk of drought
440 increases over 2 times in these catchments. Besides, we find a marked increase in the number of catchments
441 with increased drought risk compared to the univariate drought assessments. The JRP of catchments in
442 Northeastern and Central China tends to decrease, suggesting higher changes in risks than univariate
443 assessments. This result is consistent with previous studies (He et al., 2011; Xu et al., 2015), which indicates
444 that the use of bivariate drought analysis can synthesize the effects of two drought characteristics.

445 Future GDP and population exposed to increasing bivariate drought risk under three scenarios are shown
446 in [Figure 12](#). The eastern coastal regions have a higher significant economic exposure such as the Huaihe



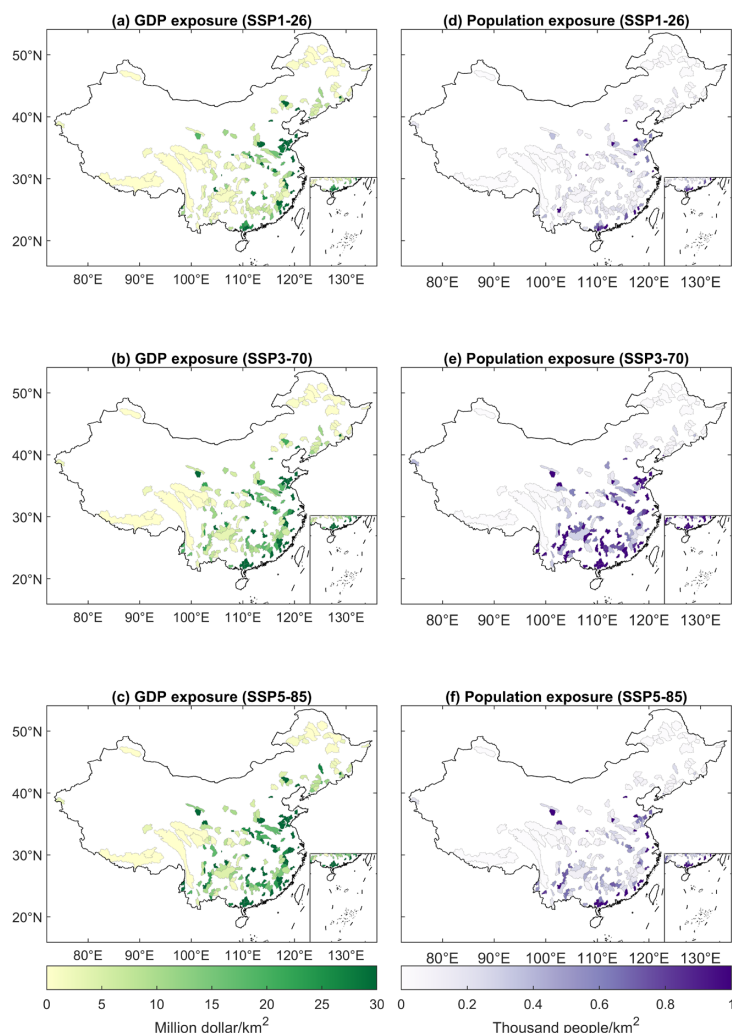
447 River Basin, the Yangtze River Basin and the Pearl River Basin, which is consistent with the distribution of
448 economically developed regions in China. The medians of GDP exposure are 5.5, 9.8 and 14.3 million
449 dollars/km² under three SSPs respectively, which indicates the vulnerability of economic losses to drought
450 disasters under global warming. The population affected by drought is mainly located in the southern Yangtze
451 River Basin and the Huaihe River Basin under SSP3-70, as the median exposure is 525 and 205 people/km²
452 under SSP3-70 and SSP5-85, respectively. This is because the increase in population is higher in the Sichuan,
453 Guangdong and Zhejiang provinces than in other Chinese provinces under SSP3-70 (Chen et al., 2020).
454 Overall, the exposure of GDP and population shows large heterogeneity in their sensitivity to different
455 scenarios, and the distribution of the affected catchments is consistent with economic and social development.



456

457 **Figure 11. The future multi-model ensemble means JRP of the historical drought with a 50-year RP based on**
458 **the bivariate approach. The future JRPs of 179 catchments under three SSPs are presented in (a)-(c), while (d)**
459 **displays raincloud plots of the projected JRP under each SSP.**

460



461

462 **Figure 12. The multi-model ensemble means exposure of GDP (a-c) and population (d-f) to bivariate drought**
463 **characteristics under different SSPs in the future period.**

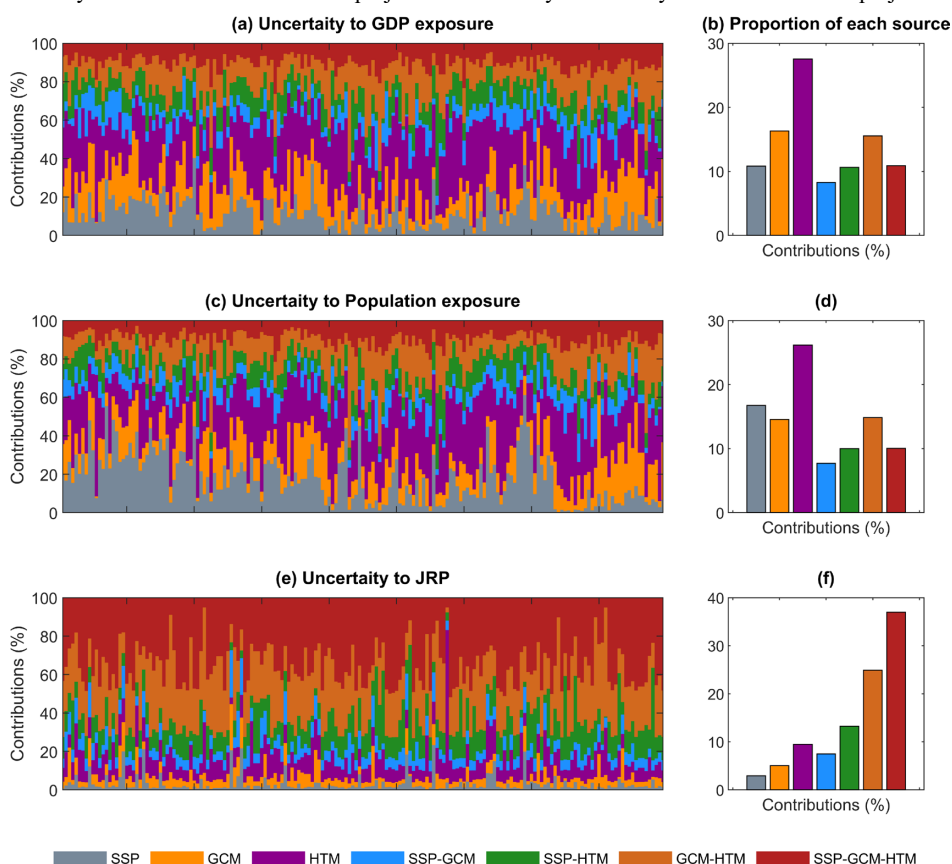
464 5. Discussion

465 5.1 Uncertainty decomposition

466 The overall uncertainty in our projections arises from the different SSPs, GCMs and HTMs as well as
467 their interactions. We assemble these seven sources using MANOVA (Figure 13). For GDP and POP exposure,
468 we find HTM is the main source of uncertainty, and contributes 27.55% and 26.14% uncertainty, respectively.
469 This indicates that the quality of the HTM is important for the accuracy of socioeconomic predictions.
470 Likewise, the GCM and GCM-HTM provide over 30% of the uncertainty in GDP and population exposures,



471 which indicates the critical importance of bias-corrected GCM outputs for accurate projections. Further, the
 472 contributions of the SSPs to population exposure is 1.5 times than that of GDP exposure, which shows that
 473 the effect of climate change is greater for POP exposure than GDP exposure. In particular, the independent
 474 factors (i.e., SSP, GCM, HTM) contribute over 50% to the uncertainty of GDP and population exposures,
 475 suggesting that GDP and population exposures are less responsive to complex coupling. In contrast, the
 476 coupled factors (i.e., the combination of SSP, GCM or HTM) mainly contribute to the uncertainty of the JRP,
 477 accounting for 82.63% of the overall uncertainty, especially the SSM-GCM-HTM, which accounts for 36.97%
 478 of uncertainty. Finally, the relatively low contribution of the choice of SSP, SSP-GCM and SSP-HTM to JRP
 479 uncertainty indicates that the future risk projection uncertainty is relatively stable in future risk projections



480
 481 **Figure 13.** The fractional uncertainty contributions of all sources to the GDP exposure, population exposure, and
 482 JRP estimate for all 179 catchments (a, c, e) and the average fractional contribution of each source (b, d, f).

483 5.2 Limitations and future work

484 As hydrological drought is a complex weather-related hazard influenced by both nature and human
 485 intervention, further work is still required to reveal the principles of drought generation. Although the hybrid
 486 models show good performance in streamflow simulation over the selected period, the underlying uncertainty



487 and the coupling relationships behind interrelated variables remain unexplained in this study. Therefore, the
488 study of the interactions among data sources is important to reveal the drivers affecting the water cycle under
489 climate change. Here, only five GCM outputs and one in situ observation dataset were used to drive our HTM
490 models. The sparse dataset may undermine the robustness of the approach, particularly when attempting to
491 simulate extreme drought events (e.g., the extreme drought in the Yangtze River Basin in 2022). Although
492 the machine learning model show good performance herein, significantly reducing the reliance on
493 observational data, continuous streamflow observations are still important to improve model accuracy.
494 Providing a larger number of GCMs and observational data to assemble a more sophisticated model might
495 be an effective approach to improve the accuracy and reliability of the model. Finally, the GDP and population
496 projections cannot well reflect future economic development and population migration. In particular,
497 government interference in immigration policies is likely to lead to large uncertainties in the projections.
498 Therefore, considering the dynamic impact of human management on socioeconomic development is
499 essential for the construction of a reliable projection framework.

500 **5.3 Suggestions for drought mitigation in China**

501 In order to curb global warming and mitigate the threats by climate change, the Chinese government is
502 striving to reach its carbon peak before 2030, achieve carbon neutrality before 2060, and bolster efforts in
503 disaster reduction (Kundzewicz et al., 2019; Liu et al., 2022b). China has nonetheless experienced several
504 extreme drought events during the past 5 years, threatening the population's health and economic
505 development. (Ding and Gao, 2020; Mallapaty, 2022; Liu et al., 2022a) The Intergovernmental Panel on
506 Climate Change (IPCC) has emphasized that projections of future climate trends can equip policymakers
507 with the scientific insight needed to navigate the challenges of climate change (Pörtner et al., 2022). The
508 results of this study aim to alert policymakers to drought risk in Southwestern China, which is expected to
509 intensify with climate change. Preserving local ecological balance and employing rational use of water
510 resources could be the key in mitigating potential losses from extreme droughts (Sohn et al., 2016; Chang et
511 al., 2019). Finally, this work highlights the importance of strictly implementing carbon emission reduction
512 initiatives and developing prevention programs to limit potential drought losses.

513 **6. Conclusions**

514 In this study, the hybrid LSTM-constrained hydrological models show high accuracy in studied
515 catchments over China, demonstrating that machine learning can effectively constrain the hydrological
516 projections. Projected changes in 50-year bivariate drought characteristics, expressed as a JRP, indicate that
517 the risk of hydrological drought is likely to more than double in over 60% of catchments by the end of the
518 21st century under SSP5-85. The spatial distribution of change reveals that the catchments with severely
519 increased drought risk are mainly located in southwestern China. Notably, the exposure of GDP and
520 population varies greatly across different SSPs. The median GDP exposure under SSP5-85 is 1.5 times that



521 of SSP3-70, but the median population exposure is just 40% that of SSP3-70. The higher population exposure
522 under SSP3-70 can be attributed to rapid population growth. Finally, we find the interaction between multiple
523 sources of data explains more than 80% of the uncertainty in future changes in JRPs, showing the importance
524 of considering the relationships between model components. Our findings demonstrate that China is facing
525 a high risk of drought under climate change and rising pressures on population and economic growth,
526 emphasizing the urgency of achieving carbon neutrality goals and implementing strategies to reduce carbon
527 emissions.

528

529 **Data availability**

530

531 The gridded meteorological dataset for China can be obtained from <http://www.cma.gov.cn>. The
532 ISIMIP3b data can be downloaded from <https://data.isimip.org>. The ERA5-Land data can be
533 downloaded from <https://www.ecmwf.int/en/era5-land>. Streamflow simulations used in this study
534 are available at <https://osf.io/fvyse/>.

535 **Acknowledgments**

536 J.Y. acknowledges support from the National Natural Science Foundation of China (Grant NOs.
537 52009091; 52242904; 52261145744) and the Fundamental Research Funds for the Central Universities
538 (NO. 2042022kf1221). L.S. is supported by UKRI (MR/V022008/1). J.G. is supported by the National
539 Natural Science Foundation of China (NO. 52179018). This work is also supported by the
540 Undergraduate Training Programs for Innovation and Entrepreneurship of Wuhan University. The
541 numerical calculations in this paper have been performed on the supercomputing system in the
542 Supercomputing Center of Wuhan University.

543 **Competing interests**

544 At least one of the (co-)authors is a member of the editorial board of Hydrology and Earth System
545 Sciences.

546 **References**

- 547 Allan, R. P., Barlow, M., Byrne, M. P., Cherchi, A., Douville, H., Fowler, H. J., Gan, T. Y., Pendergrass,
548 A. G., Rosenfeld, D., Swann, A. L. S., Wilcox, L. J., and Zolina, O.: Advances in understanding
549 large-scale responses of the water cycle to climate change, *Annals of the New York Academy of
550 Sciences*, 1472, 49–75, <https://doi.org/10.1111/nyas.14337>, 2020.
- 551 Antoniadis, A., Lambert-Lacroix, S., and Poggi, J.-M.: Random forests for global sensitivity analysis: A
552 selective review, *Reliability Engineering & System Safety*, 206, 107312, 2021.
- 553 Arsenault, R., Essou, G. R., and Brissette, F. P.: Improving hydrological model simulations with combined
554 multi-input and multimodel averaging frameworks, *Journal of Hydrologic Engineering*, 22, 04016066,
555 2017.
- 556 Ashrafi, S. M., Gholami, H., and Najafi, M. R.: Uncertainties in runoff projection and hydrological drought
557 assessment over Gharezu basin under CMIP5 RCP scenarios, *Journal of Water and Climate Change*,
558 11, 145–163, 2020.
- 559 Ayantobo, O. O., Li, Y., Song, S., and Yao, N.: Spatial comparability of drought characteristics and related
560 return periods in mainland China over 1961–2013, *Journal of Hydrology*, 550, 549–567, 2017.
- 561 Barker, L. J., Hannaford, J., Chiveron, A., and Svensson, C.: From meteorological to hydrological drought



- 562 using standardised indicators, *Hydrology and Earth System Sciences*, 20, 2483–2505, 2016.
- 563 Bergström, S.: The HBV model, *Computer models of watershed hydrology*, 443–476, 1995.
- 564 BERGSTRÖM, S. and FORSMAN, A.: DEVELOPMENT OF A CONCEPTUAL DETERMINISTIC
- 565 RAINFALL-RUNOFF MODEL, *Hydrology Research*, 4, 147–170, 1973.
- 566 Berne, A., Delrieu, G., Creutin, J.-D., and Obled, C.: Temporal and spatial resolution of rainfall
- 567 measurements required for urban hydrology, *Journal of Hydrology*, 299, 166–179, 2004.
- 568 Byakatonda, J., Parida, B. P., Moalafhi, D. B., and Kenabatho, P. K.: Analysis of long term drought
- 569 severity characteristics and trends across semiarid Botswana using two drought indices, *Atmospheric*
- 570 *research*, 213, 492–508, 2018.
- 571 Castle, S. L., Thomas, B. F., Reager, J. T., Rodell, M., Swenson, S. C., and Famiglietti, J. S.: Groundwater
- 572 depletion during drought threatens future water security of the Colorado River Basin, *Geophysical*
- 573 *research letters*, 41, 5904–5911, 2014.
- 574 Chang, J., Guo, A., Wang, Y., Ha, Y., Zhang, R., Xue, L., and Tu, Z.: Reservoir operations to mitigate
- 575 drought effects with a hedging policy triggered by the drought prevention limiting water level, *Water*
- 576 *Resources Research*, 55, 904–922, 2019.
- 577 Chen, H. and Sun, J.: Increased population exposure to extreme droughts in China due to 0.5 °C of
- 578 additional warming, *Environ. Res. Lett.*, 14, 064011, <https://doi.org/10.1088/1748-9326/ab072e>, 2019.
- 579 Chen, J., Li, C., Brissette, F. P., Chen, H., Wang, M., and Essou, G. R.: Impacts of correcting the inter-
- 580 variable correlation of climate model outputs on hydrological modeling, *Journal of hydrology*, 560,
- 581 326–341, 2018.
- 582 Chen, Y., Guo, F., Wang, J., Cai, W., Wang, C., and Wang, K.: Provincial and gridded population
- 583 projection for China under shared socioeconomic pathways from 2010 to 2100, *Scientific Data*, 7, 83,
- 584 <https://doi.org/10.1038/s41597-020-0421-y>, 2020.
- 585 Chen, Z. and Yang, G.: Analysis of drought hazards in North China: distribution and interpretation, *Nat*
- 586 *Hazards*, 65, 279–294, <https://doi.org/10.1007/s11069-012-0358-3>, 2013.
- 587 Chiew, F. H. S., Peel, M. C., and Western, A. W.: Application and testing of the simple rainfall-runoff
- 588 model SIMHYD., *Mathematical models of small watershed hydrology and applications*, 335–367,
- 589 2002.
- 590 Cho, K., Van Merriënboer, B., Gulcehre, C., Bahdanau, D., Bougares, F., Schwenk, H., and Bengio, Y.:
591 Learning phrase representations using RNN encoder-decoder for statistical machine translation, *arXiv*
- 592 preprint arXiv:1406.1078, 2014.
- 593 Chowdary, J. S., Hu, K., Srinivas, G., Kosaka, Y., Wang, L., and Rao, K. K.: The Eurasian jet streams as
- 594 conduits for East Asian monsoon variability, *Current Climate Change Reports*, 5, 233–244, 2019.
- 595 Dai, A., Zhao, T., and Chen, J.: Climate Change and Drought: a Precipitation and Evaporation Perspective,
- 596 *Curr Clim Change Rep*, 4, 301–312, <https://doi.org/10.1007/s40641-018-0101-6>, 2018.
- 597 Dikici, M.: Drought analysis with different indices for the Asi Basin (Turkey), *Sci Rep*, 10, 20739,
- 598 <https://doi.org/10.1038/s41598-020-77827-z>, 2020.
- 599 Dikshit, A., Pradhan, B., and Huete, A.: An improved SPEI drought forecasting approach using the long
- 600 short-term memory neural network, *Journal of environmental management*, 283, 111979, 2021a.
- 601 Dikshit, A., Pradhan, B., and Alamri, A. M.: Long lead time drought forecasting using lagged climate
- 602 variables and a stacked long short-term memory model, *Science of The Total Environment*, 755,
- 603 142638, 2021b.
- 604 Ding, T. and Gao, H.: The record-breaking extreme drought in Yunnan Province, Southwest China during
- 605 spring-early summer of 2019 and possible causes, *Journal of Meteorological Research*, 34, 997–1012,
- 606 2020.
- 607 Dixit, S., Atla, B. M., and Jayakumar, K. V.: Evolution and drought hazard mapping of future
- 608 meteorological and hydrological droughts using CMIP6 model, *Stochastic Environmental Research*
- 609 *and Risk Assessment*, 36, 3857–3874, 2022.
- 610 Donat, M. G., Lowry, A. L., Alexander, L. V., O’Gorman, P. A., and Maher, N.: More extreme
- 611 precipitation in the world’s dry and wet regions, *Nature Climate Change*, 6, 508–513, 2016.
- 612 Duan, Q., Sorooshian, S., and Gupta, V.: Effective and efficient global optimization for conceptual rainfall-
- 613 runoff models, , 28, 1015–1031, 1992.
- 614 Fujimori, S., Hasegawa, T., Masui, T., Takahashi, K., Herran, D. S., Dai, H., Hijioka, Y., and Kainuma, M.:
615 SSP3: AIM implementation of shared socioeconomic pathways, *Global Environmental Change*, 42,
- 616 268–283, 2017.



- 617 Ganguli, P. and Merz, B.: Trends in compound flooding in northwestern Europe during 1901–2014,
618 *Geophysical Research Letters*, 46, 10810–10820, 2019.
- 619 Gers, F. A., Schmidhuber, J., and Cummins, F.: Learning to forget: continual prediction with LSTM,
620 *Neural Comput*, 12, 2451–71, 2000.
- 621 Green, J. K., Berry, J., Ciais, P., Zhang, Y., and Gentine, P.: Amazon rainforest photosynthesis increases in
622 response to atmospheric dryness, *Science Advances*, 6, eabb7232, 2020.
- 623 Gu, L., Chen, J., Yin, J., Sullivan, S. C., Wang, H.-M., Guo, S., Zhang, L., and Kim, J.-S.: Projected
624 increases in magnitude and socioeconomic exposure of global droughts in 1.5 and 2°C
625 warmer climates, *Hydrology and Earth System Sciences*, 24, 451–472, [https://doi.org/10.5194/hess-](https://doi.org/10.5194/hess-24-451-2020)
626 [24-451-2020](https://doi.org/10.5194/hess-24-451-2020), 2020a.
- 627 Gu, L., Chen, J., Yin, J., Xu, C.-Y., and Zhou, J.: Responses of precipitation and runoff to climate warming
628 and implications for future drought changes in China, *Earth’s Future*, 8, e2020EF001718, 2020b.
- 629 Gu, L., Yin, J., Zhang, H., Wang, H.-M., Yang, G., and Wu, X.: On future flood magnitudes and estimation
630 uncertainty across 151 catchments in mainland China, *International Journal of Climatology*, 41, E779–
631 E800, 2021.
- 632 Gu, L., Yin, J., Wang, S., Chen, J., Qin, H., Yan, X., He, S., and Zhao, T.: How well do the multi-satellite
633 and atmospheric reanalysis products perform in hydrological modelling, *Journal of Hydrology*, 617,
634 128920, <https://doi.org/10.1016/j.jhydrol.2022.128920>, 2023.
- 635 He, B., Lü, A., Wu, J., Zhao, L., and Liu, M.: Drought hazard assessment and spatial characteristics
636 analysis in China, *Journal of Geographical Sciences*, 21, 235–249, 2011.
- 637 Hu, C., Guo, S., Xiong, L., and Peng, D.: A modified Xinanjiang model and its application in northern
638 China, *Hydrology Research*, 36, 175–192, 2005.
- 639 Jiang, T., Jing, Z., Cheng, J., Lige, C., Yanjun, W., Hemin, S., Anqian, W., Jinlong, H., Buda, S., and Run,
640 W.: National and provincial population projected to 2100 under the shared socioeconomic pathways in
641 China, *Advances in Climate Change Research*, 13, 128, 2017.
- 642 Jiang, T., Jing, Z., Li-Ge, C. A. O., Yan-Jun, W., Bu-Da, S. U., Cheng, J., Run, W., and Chao, G. A. O.:
643 Projection of national and provincial economy under the shared socioeconomic pathways in China,
644 *Advances in Climate Change Research*, 14, 50, 2018.
- 645 Kim, J. H., Sung, J. H., Chung, E.-S., Kim, S. U., Son, M., and Shiru, M. S.: Comparison of Projection in
646 Meteorological and Hydrological Droughts in the Cheongmicheon Watershed for RCP4. 5 and SSP2-
647 4.5, *Sustainability*, 13, 2066, 2021.
- 648 Koutsoyiannis, D.: Clausius–Clapeyron equation and saturation vapour pressure: simple theory reconciled
649 with practice, *European Journal of physics*, 33, 295, 2012.
- 650 Kriauciuniene, J., Jakimavicius, D., Sarauskiene, D., and Kaliatka, T.: Estimation of uncertainty sources in
651 the projections of Lithuanian river runoff, *Stochastic Environmental Research and Risk Assessment*,
652 27, 769–784, 2013.
- 653 Kumar, R., Musuza, J. L., Van Loon, A. F., Teuling, A. J., Barthel, R., Ten Broek, J., Mai, J., Samaniego,
654 L., and Attinger, S.: Multiscale evaluation of the Standardized Precipitation Index as a groundwater
655 drought indicator, *Hydrology and Earth System Sciences*, 20, 1117–1131, 2016.
- 656 Kundzewicz, Z., Su, B., Wang, Y., Xia, J., Huang, J., and Jiang, T.: Flood risk and its reduction in China,
657 *Advances in Water Resources*, 130, 37–45, <https://doi.org/10.1016/j.advwatres.2019.05.020>, 2019.
- 658 Kunnath-Poovakka, A. and Eldho, T. I.: A comparative study of conceptual rainfall-runoff models GR4J,
659 AWBM and Sacramento at catchments in the upper Godavari river basin, India, *J Earth Syst Sci*, 128,
660 33, <https://doi.org/10.1007/s12040-018-1055-8>, 2019.
- 661 Lange, S.: Trend-preserving bias adjustment and statistical downscaling with ISIMIP3BASD (v1.0),
662 *Geoscientific Model Development*, 12, 3055–3070, <https://doi.org/10.5194/gmd-12-3055-2019>, 2019.
- 663 Li, D. X.: On default correlation: A copula function approach, Available at SSRN 187289,
664 <https://doi.org/10.2139/ssrn.187289>, 1999.
- 665 Liu, J., Zhang, Q., Singh, V. P., and Shi, P.: Contribution of multiple climatic variables and human
666 activities to streamflow changes across China, *Journal of Hydrology*, 545, 145–162,
667 <https://doi.org/10.1016/j.jhydrol.2016.12.016>, 2017.
- 668 Liu, Y., Hu, Z.-Z., Wu, R., and Yuan, X.: Causes and predictability of the 2021 spring southwestern China
669 severe drought, *Advances in Atmospheric Sciences*, 39, 1766–1776, 2022a.
- 670 Liu, Z., Deng, Z., He, G., Wang, H., Zhang, X., Lin, J., Qi, Y., and Liang, X.: Challenges and opportunities
671 for carbon neutrality in China, *Nat Rev Earth Environ*, 3, 141–155, <https://doi.org/10.1038/s43017->



- 672 021-00244-x, 2022b.
- 673 Lu, R., Xu, K., Chen, R., Chen, W., Li, F., and Lv, C.: Heat waves in summer 2022 and increasing concern
674 regarding heat waves in general, *Atmospheric and Oceanic Science Letters*, 16, 100290,
675 <https://doi.org/10.1016/j.aosl.2022.100290>, 2023.
- 676 Ma, N., Szilagyi, J., Zhang, Y., and Liu, W.: Complementary-Relationship-Based Modeling of Terrestrial
677 Evapotranspiration Across China During 1982–2012: Validations and Spatiotemporal Analyses,
678 *Journal of Geophysical Research: Atmospheres*, 124, 4326–4351,
679 <https://doi.org/10.1029/2018JD029850>, 2019.
- 680 Mallapaty, S.: China’s extreme weather challenges scientists studying it, *Nature*, 609, 888, 2022.
- 681 Martel, J., Demeester, K., Brissette, F., Poulin, A., and Arsenault, R.: HMETS-A simple and efficient
682 hydrology model for teaching hydrological modelling, flow forecasting and climate change impacts,
683 *International Journal of Engineering Education*, 2017.
- 684 Meinshausen, M., Nicholls, Z. R., Lewis, J., Gidden, M. J., Vogel, E., Freund, M., Beyerle, U., Gessner, C.,
685 Nauels, A., and Bauer, N.: The shared socio-economic pathway (SSP) greenhouse gas concentrations
686 and their extensions to 2500, *Geoscientific Model Development*, 13, 3571–3605, 2020.
- 687 Mokhtar, A., Jalali, M., He, H., Al-Ansari, N., Elbeltagi, A., Alsafadi, K., Abdo, H. G., Sammen, S. S.,
688 Gyasi-Agyei, Y., and Rodrigo-Comino, J.: Estimation of SPEI meteorological drought using machine
689 learning algorithms, *IEEE Access*, 9, 65503–65523, 2021.
- 690 Myronidis, D., Ioannou, K., Fotakis, D., and Dörflinger, G.: Streamflow and hydrological drought trend
691 analysis and forecasting in Cyprus, *Water resources management*, 32, 1759–1776, 2018.
- 692 Nabaei, S., Sharafati, A., Yaseen, Z. M., and Shahid, S.: Copula based assessment of meteorological
693 drought characteristics: regional investigation of Iran, *Agricultural and Forest Meteorology*, 276,
694 107611, 2019.
- 695 Nie, N., Zhang, W., Chen, H., and Guo, H.: A global hydrological drought index dataset based on gravity
696 recovery and climate experiment (GRACE) data, *Water Resources Management*, 32, 1275–1290,
697 2018.
- 698 O’Neill, B. C., Tebaldi, C., Van Vuuren, D. P., Eyring, V., Friedlingstein, P., Hurtt, G., Knutti, R.,
699 Krieger, E., Lamarque, J.-F., and Lowe, J.: The scenario model intercomparison project
700 (ScenarioMIP) for CMIP6, *Geoscientific Model Development*, 9, 3461–3482, 2016.
- 701 Oudin, L., Hervieu, F., Michel, C., Perrin, C., Andréassian, V., Anctil, F., and Loumagne, C.: Which
702 potential evapotranspiration input for a lumped rainfall–runoff model?: Part 2—Towards a simple and
703 efficient potential evapotranspiration model for rainfall–runoff modelling, *Journal of Hydrology*, 303,
704 290–306, 2005.
- 705 Pelosi, A., Terribile, F., D’Urso, G., and Chirico, G. B.: Comparison of ERA5-Land and UERRA
706 MESCAN-SURFEX reanalysis data with spatially interpolated weather observations for the regional
707 assessment of reference evapotranspiration, *Water*, 12, 1669, 2020.
- 708 Perrin, C., Michel, C., and Andréassian, V.: Improvement of a parsimonious model for streamflow
709 simulation, *Journal of hydrology*, 279, 275–289, 2003.
- 710 Piao, S., Ciais, P., Huang, Y., Shen, Z., Peng, S., Li, J., Zhou, L., Liu, H., Ma, Y., Ding, Y., Friedlingstein,
711 P., Liu, C., Tan, K., Yu, Y., Zhang, T., and Fang, J.: The impacts of climate change on water resources
712 and agriculture in China, *Nature*, 467, 43–51, <https://doi.org/10.1038/nature09364>, 2010.
- 713 Pokhrel, Y., Felfelani, F., Satoh, Y., Boulange, J., Burek, P., Gädeke, A., Gerten, D., Gosling, S. N.,
714 Grillakis, M., and Gudmundsson, L.: Global terrestrial water storage and drought severity under
715 climate change, *Nature Climate Change*, 11, 226–233, 2021.
- 716 Porter, J. W. and McMahon, T. A.: Application of a catchment model in southeastern Australia, *Journal of*
717 *Hydrology*, 24, 121–134, 1975.
- 718 Pörtner, H.-O., Roberts, D. C., Poloczanska, E. S., Mintenbeck, K., Tignor, M., Alegría, A., Craig, M.,
719 Langsdorf, S., Löschke, S., and Möller, V.: IPCC, 2022: Summary for policymakers, 2022.
- 720 Qi, W., Chen, J., Li, L., Xu, C., Li, J., Xiang, Y., and Zhang, S.: A framework to regionalize conceptual
721 model parameters for global hydrological modeling, *Hydrology and Earth System Sciences*
722 *Discussions*, 1–28, <https://doi.org/10.5194/hess-2020-127>, 2020.
- 723 Rahmati, O., Falah, F., Dayal, K. S., Deo, R. C., Mohammadi, F., Biggs, T., Moghaddam, D. D., Naghibi,
724 S. A., and Bui, D. T.: Machine learning approaches for spatial modeling of agricultural droughts in the
725 south-east region of Queensland Australia, *Science of the Total Environment*, 699, 134230, 2020.
- 726 Ren-Jun, Z.: The Xinanjiang model applied in China, *Journal of hydrology*, 135, 371–381, 1992.



- 727 Schmidt, R., Schwintzer, P., Flechtner, F., Reigber, C., Güntner, A., Döll, P., Ramillien, G., Cazenave, A.,
728 Petrovic, S., and Jochmann, H.: GRACE observations of changes in continental water storage, *Global*
729 *and Planetary Change*, 50, 112–126, 2006.
- 730 Sherstinsky, A.: Fundamentals of recurrent neural network (RNN) and long short-term memory (LSTM)
731 network, *Physica D: Nonlinear Phenomena*, 404, 132306, 2020.
- 732 Shin, M.-J. and Kim, C.-S.: Component combination test to investigate improvement of the IHACRES and
733 GR4J rainfall–runoff models, *Water*, 13, 2126, 2021.
- 734 Shukla, S. and Wood, A. W.: Use of a standardized runoff index for characterizing hydrologic drought,
735 *Geophysical research letters*, 35, 2008.
- 736 Simmons, A. J., Untch, A., Jakob, C., Kållberg, P., and Undén, P.: Stratospheric water vapour and tropical
737 tropopause temperatures in Ecmwf analyses and multi-year simulations, , 125, 353–386, 1999.
- 738 Sohn, J. A., Saha, S., and Bauhus, J.: Potential of forest thinning to mitigate drought stress: A meta-
739 analysis, *Forest Ecology and Management*, 380, 261–273,
740 <https://doi.org/10.1016/j.foreco.2016.07.046>, 2016.
- 741 Sönmez, A. Y. and Kale, S.: Climate change effects on annual streamflow of Filyos River (Turkey),
742 *Journal of Water and Climate Change*, 11, 420–433, <https://doi.org/10.2166/wcc.2018.060>, 2018.
- 743 Stewart, I. T.: Changes in snowpack and snowmelt runoff for key mountain regions, *Hydrological*
744 *Processes*, 23, 78–94, <https://doi.org/10.1002/hyp.7128>, 2009.
- 745 Su, B., Huang, J., Fischer, T., Wang, Y., Kundzewicz, Z. W., Zhai, J., Sun, H., Wang, A., Zeng, X., and
746 Wang, G.: Drought losses in China might double between the 1.5 C and 2.0 C warming, *Proceedings*
747 *of the National Academy of Sciences*, 115, 10600–10605, 2018.
- 748 Tabari, H.: Climate change impact on flood and extreme precipitation increases with water availability,
749 *Scientific reports*, 10, 1–10, 2020.
- 750 Tapley, B. D., Bettadpur, S., Ries, J. C., Thompson, P. F., and Watkins, M. M.: GRACE measurements of
751 mass variability in the Earth system, *science*, 305, 503–505, 2004.
- 752 Tian, Y., Xu, Y.-P., and Zhang, X.-J.: Assessment of Climate Change Impacts on River High Flows
753 through Comparative Use of GR4J, HBV and Xinanjiang Models, *Water Resources Management*, 27,
754 2871–2888, 2013.
- 755 Tirivarombo, S., Osupile, D., and Eliasson, P.: Drought monitoring and analysis: standardised precipitation
756 evapotranspiration index (SPEI) and standardised precipitation index (SPI), *Physics and Chemistry of*
757 *the Earth, Parts A/B/C*, 106, 1–10, 2018.
- 758 Udall, B. and Overpeck, J.: The twenty-first century Colorado River hot drought and implications for the
759 future, *Water Resources Research*, 53, 2404–2418, 2017.
- 760 Vicente-Serrano, S. M., López-Moreno, J. I., Beguería, S., Lorenzo-Lacruz, J., Azorin-Molina, C., and
761 Morán-Tejeda, E.: Accurate computation of a streamflow drought index, *Journal of Hydrologic*
762 *Engineering*, 17, 318–332, 2012.
- 763 Wang, Z., Li, J., Lai, C., Zeng, Z., Zhong, R., Chen, X., Zhou, X., and Wang, M.: Does drought in China
764 show a significant decreasing trend from 1961 to 2009?, *Science of The Total Environment*, 579, 314–
765 324, <https://doi.org/10.1016/j.scitotenv.2016.11.098>, 2017.
- 766 Weinfurt, K. P.: Multivariate analysis of variance, in: *Reading and understanding multivariate statistics*,
767 *American Psychological Association*, Washington, DC, US, 245–276, 1995.
- 768 Woolway, R. I., Kraemer, B. M., Lenters, J. D., Merchant, C. J., O’Reilly, C. M., and Sharma, S.: Global
769 lake responses to climate change, *Nat Rev Earth Environ*, 1, 388–403, <https://doi.org/10.1038/s43017-020-0067-5>, 2020.
- 770
- 771 Wu, J., Chen, X., Yao, H., and Zhang, D.: Multi-timescale assessment of propagation thresholds from
772 meteorological to hydrological drought, *Science of the Total Environment*, 765, 144232, 2021.
- 773 Wu, X., Guo, S., Yin, J., Yang, G., Zhong, Y., and Liu, D.: On the event-based extreme precipitation across
774 China: Time distribution patterns, trends, and return levels, *Journal of hydrology*, 562, 305–317, 2018.
- 775 Xiuja, C., Guanghua, Y., Jian, G., Ningning, M., and Zihao, W.: Application of WNN-PSO model in
776 drought prediction at crop growth stages: A case study of spring maize in semi-arid regions of
777 northern China, *Computers and Electronics in Agriculture*, 199, 107155, 2022.
- 778 Xu, K., Yang, D., Yang, H., Li, Z., Qin, Y., and Shen, Y.: Spatio-temporal variation of drought in China
779 during 1961–2012: A climatic perspective, *Journal of Hydrology*, 526, 253–264, 2015.
- 780 Yao, F., Livneh, B., Rajagopalan, B., Wang, J., Crétaux, J.-F., Wada, Y., and Berge-Nguyen, M.: Satellites
781 reveal widespread decline in global lake water storage, *Science*, 380, 743–749,



- 782 <https://doi.org/10.1126/science.abo2812>, 2023.
783 Yevjevich, V. M.: Objective approach to definitions and investigations of continental hydrologic droughts,
784 An, PhD Thesis, Colorado State University. Libraries, 1967.
785 Yihdego, Y., Vaheddoost, B., and Al-Weshah, R. A.: Drought indices and indicators revisited, Arab J
786 Geosci, 12, 69, <https://doi.org/10.1007/s12517-019-4237-z>, 2019.
787 Yilmaz, M.: Accuracy assessment of temperature trends from ERA5 and ERA5-Land, Science of The Total
788 Environment, 856, 159182, <https://doi.org/10.1016/j.scitotenv.2022.159182>, 2023.
789 Yin, J., Guo, S., He, S., Guo, J., Hong, X., and Liu, Z.: A copula-based analysis of projected climate
790 changes to bivariate flood quantiles, Journal of hydrology, 566, 23–42, 2018.
791 Yin, J., Guo, S., Gu, L., He, S., Ba, H., Tian, J., Li, Q., and Chen, J.: Projected changes of bivariate flood
792 quantiles and estimation uncertainty based on multi-model ensembles over China, Journal of
793 Hydrology, 585, 124760, 2020.
794 Yin, J., Guo, S., Gu, L., Zeng, Z., Liu, D., Chen, J., Shen, Y., and Xu, C.-Y.: Blending multi-satellite,
795 atmospheric reanalysis and gauge precipitation products to facilitate hydrological modelling, Journal
796 of Hydrology, 593, 125878, 2021a.
797 Yin, J., Guo, S., Gentine, P., Sullivan, S. C., Gu, L., He, S., Chen, J., and Liu, P.: Does the hook structure
798 constrain future flood intensification under anthropogenic climate warming?, Water Resources
799 Research, 57, e2020WR028491, 2021b.
800 Yin, J., Guo, S., Yang, Y., Chen, J., Gu, L., Wang, J., He, S., Wu, B., and Xiong, J.: Projection of droughts
801 and their socioeconomic exposures based on terrestrial water storage anomaly over China, Sci. China
802 Earth Sci., 65, 1772–1787, <https://doi.org/10.1007/s11430-021-9927-x>, 2022.
803 Yin, J., Gentine, P., Slater, L., Gu, L., Pokhrel, Y., Hanasaki, N., Guo, S., Xiong, L., and Schlenker, W.:
804 Future socio-ecosystem productivity threatened by compound drought–heatwave events, Nat Sustain,
805 6, 259–272, <https://doi.org/10.1038/s41893-022-01024-1>, 2023.
806 Yu, B. and Zhu, Z.: A comparative assessment of AWBM and SimHyd for forested watersheds,
807 Hydrological sciences journal, 60, 1200–1212, 2015.
808 Yu, Y., Si, X., Hu, C., and Zhang, J.: A Review of Recurrent Neural Networks: LSTM Cells and Network
809 Architectures, Neural Comput, 31, 1235–1270, 2019.
810 Zhai, P. M. and Zou, X. K.: Changes in temperature and precipitation and their impacts on drought in
811 China during 1951–2003, Advances in Climate Change Research, 1, 16–18, 2005.
812 Zhang, F., Deng, X., Xie, L., and Xu, N.: China’s energy-related carbon emissions projections for the
813 shared socioeconomic pathways, Resources, Conservation and Recycling, 168, 105456, 2021.
814 Zhang, G., Gan, T. Y., and Su, X.: Twenty-first century drought analysis across China under climate
815 change, Climate Dynamics, 59, 1665–1685, 2022.
816 Zhao, M., A. G., Velicogna, I., and Kimball, J. S.: Satellite Observations of Regional Drought Severity in
817 the Continental United States Using GRACE-Based Terrestrial Water Storage Changes, Journal of
818 Climate, 30, 6297–6308, <https://doi.org/10.1175/JCLI-D-16-0458.1>, 2017.
819 Zheng, J., Wang, H., and Liu, B.: Impact of the long-term precipitation and land use changes on runoff
820 variations in a humid subtropical river basin of China, Journal of Hydrology: Regional Studies, 42,
821 101136, 2022.
822 Zhu, Q., Luo, Y., Zhou, D., Xu, Y.-P., Wang, G., and Tian, Y.: Drought prediction using in situ and remote
823 sensing products with SVM over the Xiang River Basin, China, Natural Hazards, 105, 2161–2185,
824 2021.
825